THE ASTROPHYSICAL JOURNAL, 522:1053–1068, 1999 September 10

TWO-COMPONENT THEORETICAL CHROMOSPHERE MODELS FOR K DWARFS OF DIFFERENT MAGNETIC ACTIVITY: EXPLORING THE Ca II EMISSION–STELLAR ROTATION RELATIONSHIP

M. CUNTZ,[1] W. RAMMACHER,[2] P. ULMSCHNEIDER,[2] Z. E. MUSIELAK,[1,2,3] AND S. H. SAAR[4]
Received 1999 January 11; accepted 1999 April 26

ABSTRACT

We compute two-component theoretical chromosphere models for K2 V stars with different levels of magnetic activity. The two components are a nonmagnetic component heated by acoustic waves and a magnetic component heated by longitudinal tube waves. The filling factor for the magnetic component is determined from an observational relationship between the measured magnetic area coverage and the stellar rotation period. We consider stellar rotation periods between 10 and 40 days. We investigate two different geometrical distributions of magnetic flux tubes: uniformly distributed tubes, and tubes arranged as a chromospheric network embedded in the nonmagnetic region. The chromosphere models are constructed by performing state-of-the-art calculations for the generation of acoustic and magnetic energy in stellar convection zones, the propagation and dissipation of this energy at the different atmospheric heights, and the formation of specific chromospheric emission lines that are then compared to the observational data. In all these steps, the two-component structure of stellar photospheres and chromospheres is fully taken into account. We find that heating and chromospheric emission is significantly increased in the magnetic component and is strongest in flux tubes that spread the least with height, expected to occur on rapidly rotating stars with high magnetic filling factors. For stars with very slow rotation, we are able to reproduce the *basal flux limit* of chromospheric emission previously identified with nonmagnetic regions. Most importantly, however, we find that the relationship between the Ca II H+K emission and the stellar rotation rate deduced from our models is consistent with the relationship given by observations.

Subject headings: line: formation — MHD — stars: activity — stars: chromospheres — stars: late-type — stars: rotation

1. INTRODUCTION

An outstanding problem in current stellar astrophysics research is to identify the physical processes responsible for heating stellar chromospheres. It is now commonly accepted that two different types of mechanisms for the chromospheric heating exist, which can broadly be classified as magnetic and acoustic heating (see reviews by Narain & Ulmschneider 1990, 1996). For the Sun and other types of stars with surface convection zones, acoustic heating has been identified as most likely responsible for balancing the "basal" flux emission. Buchholz, Ulmschneider, & Cuntz (1998, hereafter B98) have calculated acoustic heating models for inactive main-sequence stars and giants and have shown that the observed Mg II $h+k$ and Ca II H + K emission can be well reproduced by those models. Similar results but for inactive M-type dwarfs have been obtained by Mullan & Cheng (1993). So far, the most sophisticated test of the acoustic heating picture has been performed by Carlsson & Stein (1992) who found that the dissipation of acoustic wave energy in the solar chromosphere can be used to reproduce the temporal variations of the Ca II K line profile observed in the solar internetwork regions.

On the other hand, it is also well known that most, if not all, stars also exhibit magnetic activity. Thus, chromospheres of main-sequence stars are expected to consist of both magnetically and acoustically heated components. In case of the Sun, the magnetic activity is governed by the large variety of magnetic surface structures (e.g., Schrijver 1996). In various other stars, the existence of magnetic heating can directly be inferred from the observed increase of the chromospheric and transition layer emission with stellar rotation that has been found in both dwarfs (Rutten 1986, 1987; Schrijver 1987) and (sub-)giants (Rutten 1987; Rutten & Pylyser 1988; Simon & Drake 1989; Gray 1989; Strassmeier et al. 1994). Increased stellar rotation usually leads to an increased photospheric magnetic flux ($\propto B_0 f_0$), where B_0 is the photospheric magnetic field strength and f_0 is the magnetic filling factor. In fact, it is now possible to link $B_0 f_0$ to both the stellar rotation period $P_{\rm rot}$ (Marcy & Basri 1989; Montesinos & Jordan 1993; Saar 1996a; see also Cuntz, Ulmschneider, & Musielak 1998, hereafter C98) and to the emergent chromospheric emission flux (Saar & Schrijver 1987; Schrijver et al. 1989; Montesinos & Jordan 1993; Saar 1996b; Jordan 1997).

With respect to Ca II emission, a variety of studies have been done. Three decades ago, Wilson & Skumanich (1964), Wilson (1966), Kraft (1967), and others noted that chromospheric Ca II emission—known to be a proxy for magnetic activity on the Sun—was correlated with stellar age and rotation, decreasing systematically from young cluster stars to old field stars. At the time, Skumanich (1972) proposed the now famous $t^{-1/2}$ law to describe the decay of the

[1] Center for Space Plasma, Aeronomy, and Astrophysics Research (CSPAAR), University of Alabama in Huntsville, Huntsville, AL 35899; cuntzm@cspar.uah.edu.

[2] Institut für Theoretische Astrophysik, Universität Heidelberg, Tiergartenstraße 15, D-69121 Heidelberg, Germany; ulm@ita.uni-heidelberg.de.

[3] Physics Department, University of Texas at Arlington, Arlington, TX 76019; musielakz@utahep.uta.edu.

[4] Harvard-Smithsonian Center for Astrophysics, 60 Garden Street, Cambridge, MA 02138; saar@cfa.harvard.edu.

observed Ca II flux and the stellar spin. The decline in rotation was attributed to a steady loss of angular momentum in the coronal wind, itself a by-product of the activity, whereas the decrease in chromospheric activity was ascribed to a weakening of the spin-catalyzed magnetic "dynamo." Skumanich was first to realize that the link between activity and rotation is a causal one rather than given by observational coincidence. Noyes et al. (1984) identified a tight correlation between the Ca II emission and the Rossby number, a key parameter in dynamo theories (see also Jordan 1997 for details). Additional observational results were presented by Simon, Herbig, & Boesgaard (1985) and Ayres et al. (1996). The latter authors used the *Hubble Space Telescope* to observe the UV emission of solar-type stars in clusters of different ages. These observations provide strong evidence for the decay of the chromospheric and transition-layer activity with rotation rate.

Theoretical models of the long-term time evolution of dynamo action are given by Schrijver & Pols (1993), Rosner et al. (1995), Keppens, MacGregor, & Charbonneau (1995), and Charbonneau, Schrijver, & MacGregor (1997). The latter two studies contain a detailed MHD description of the time development of the internal angular momentum redistribution allowing estimates about the surface magnetic field strength and rotational velocities of main-sequence stars. These studies now provide the theoretical basis for explaining why the decrease of stellar rotation also invokes reduced values of $B_0 f_0$. If magnetic activity is concentrated within distinct active regions, and the star is not seen pole-on, rotationally modulated chromospheric emission will result (e.g., Baliunas et al. 1983, 1995; Char et al. 1993; Walter 1996). Chromospheric heating in magnetically active stars thus depends on B_0, f_0 and details of the photospheric magnetic field structure.

In our new theoretical chromospheric models, serious efforts have been made to accomplish three distinctly different steps in the modeling process, namely, to calculate the acoustic and magnetic energy generation in the stellar convection zone, to model the propagation and dissipation of acoustic and magnetic energy at different atmospheric heights, and to simulate the formation of specific chromospheric emission lines that are then compared with observations. In all these steps, the two-component structure of stellar photospheres and chromospheres is fully taken into account. The method used for calculating the acoustically heated component of stellar chromospheres is the same as that used by B98. Computation of the propagation of nonlinear and radiatively damped longitudinal tube waves in the magnetically heated component is based on previous work (see Herbold et al. 1985; Rammacher & Ulmschneider 1989; Ulmschneider, Zähringer, & Musielak 1991). Rammacher & Ulmschneider studied the formation of Ca II and Mg II emission lines inside magnetic tube waves embedded in the solar atmosphere for different wave energy fluxes and filling factors. Other results concerning the propagation and dissipation of longitudinal tube waves are described in Roberts (1991) and more recently by Bünte, Steiner, & Pizzo (1993), Steiner et al. (1996), Fawzy, Ulmschneider, & Cuntz (1998), and C98.

The main goal of this paper is to construct theoretical two-component chromosphere models for K2 V stars. These models are constructed by using newly calculated wave energy fluxes for longitudinal flux tube waves in stellar atmospheres (Ulmschneider & Musielak 1998) and our newly improved numerical codes for the wave propagation and the line formation. In the C98 paper, we discussed the basic hydrodynamic and thermodynamic properties of magnetic flux tubes in K2 V stars of different magnetic activity and thus constructed isolated flux tubes. It was assumed that the shape of these single tubes was determined by the number of flux tubes spread over the stellar surface. The number of flux tubes is given by the magnetic filling factor. In this paper, we construct models for both nonmagnetic and magnetic regions. For the latter, we consider two different cases, namely, uniformly distributed magnetic flux tubes and tubes arranged as a chromospheric network embedded in the nonmagnetic regions of stellar atmospheres. The Ca II flux resulting from these theoretical two-component chromosphere models is computed for K2 V stars of different rotation rate by using a multiray radiative transfer code. The theoretical Ca II emission–stellar rotation relationship is derived and directly compared to the observational data. Eventually, we find good agreement between the theoretical and observational relationship.

The paper is structured as follows: In § 2, we discuss the methods used. In § 3, we present our numerical results. In § 4, we discuss the comparison with observations. Conclusions are given in § 5.

2. METHOD AND MODEL ASSUMPTIONS

2.1. *Stellar Parameters and Magnetic Flux Tube Distribution*

For our K2 V star models, we take the following stellar parameters: $T_{\rm eff} = 4900$ K, $\log g_* = 4.51$ (cgs), and $R_* = 0.8\ R_\odot$. Several assumptions must be made to select properly the magnetic parameters of this star, i.e., f_0, B_0, and the shape and distribution of the magnetic flux tubes on the stellar surface. For the flux tube distribution, we consider the tubes to be arranged as a chromospheric network and to be distributed uniformly over the stellar surface. Since the tubes in the chromospheric network are more crowded than in the other case, the spreading of these tubes (i.e., the increase of their cross sections with atmospheric height) is reduced, which amplifies the local heating and in most cases also leads the enhanced radiative emission (see C98 and Fawzy et al. 1998). Nonetheless, the surface-averaged f_0 in both types of models is identical and chosen in accordance with the observational constraints discussed below.

To calculate B_0 inside the tubes at the photospheric level $\tau_{5000} = 1$, we assume approximate equipartition between the external gas pressure and magnetic pressure (e.g., Solanki 1996; Hasan & van Ballegooijen 1998) and take the gas pressure inside and outside the tube (p_i and p_e, respectively) to be related to each other by $p_i : p_e = 1:4$. The latter value has been obtained for the Sun, and it is assumed here that the same relationship holds for K2 V stars. This gives $B_0 = 2100$ G, independent of stellar rotation. As we want to construct two-component chromosphere models for stars of the same spectral type but different magnetic activity (and thereby different rotation), B_0 is constant, and so f_0 must be related to the stellar rotation period $P_{\rm rot}$. Earlier efforts to link $B_0 f_0$ to $P_{\rm rot}$ have been described by Marcy & Basri (1989), Montesinos & Jordan (1993), and others (e.g., Jordan 1997 and references therein). More recent results have shown that the previous measurements of $B_0 f_0$ were often too high by a factor of 2 or more (see

Basri, Marcy, & Valenti 1990; Saar, Bünte, & Solanki 1994; Valenti, Marcy, & Basri 1995).

In this paper, we use the $B_0 f_0$-P_{rot} relation of C98, which was derived on the basis of the most recent observational results of Rüedi et al. (1997). They present an analysis of 13 high-quality optical spectra for late-type dwarfs (G1–K5) with different rotation rates and different levels of activity. A statistical analysis of these results yields

$$B_0 f_0 = 238 - 5.51 P_{rot}$$

for 10 days $\leq P_{rot} \leq$ 50 days with B_0 in G and P_{rot} in days. This relation is strictly valid only in a statistical sense for a set of stars but may also be used to construct theoretical models for individual stars (see C98). In addition, by specifying B_0 the photospheric filling factor f_0 is directly linked to P_{rot} (see Table 1). According to the results presented in this table, both the photospheric and chromospheric magnetic filling factors, i.e., f_0 and f_N, respectively, for fast rotating stars are much larger than those for slow rotating stars. This again implies that fast rotating stars have much higher surface coverage by magnetic flux tubes than slow rotating stars.

The filling factors given in Table 1 can also be used to constrain the shape of magnetic flux tubes in stellar atmospheres. The geometrical structure of these tubes is determined in the following way. First, the diameter ($=2r_0$) of the tubes at the bottom is assumed to be equal to the local density scale height, which is 110 km, similar to that of the Sun. Second, it is assumed that the tubes spread exponentially with height between the bottom, where the wave generation takes place, and a height of 100 km (for stars with $P_{rot} = 10$ days) and 500 km (for $P_{rot} = 40$ days). This means that the interaction between the tubes in stellar atmospheres is largely negligible below the chosen heights. Hence, the filling factors determine the top opening radii of the tubes (see Table 1) for tubes embedded in atmospheres of stars with different rotation rates (see Appendix A for details). To determine the tube spreading function for the region beneath the top opening radius, we use a segment of a cosine function, which has the property of being differentiable at the fitting point. The shape of the tubes as well as the height dependence of the filling factors for different flux tube models are shown in Figures 1 and 2, respectively. At the height where the tubes merge, the filling factors are given by $\pi/4$. They are extrapolated to unity at the height $z = 1500$ km, where our calculations are terminated. This extrapolation ensures that the area between the flux tubes is also filled by magnetic fields as required by the physical picture. The type of extrapolation, however, is largely irrelevant for our models because the formation of Ca II H and K lines (i.e., the primary concern of this paper) occurs at much lower heights (see § 3 for details).

TABLE 1

FLUX TUBE PARAMETERS

P_{rot} (days)	$f_0 B_0$ (G)	f_0	f_N	f_C	r_∞ (km)
Network Tubes					
10.....	183	0.087	0.348	0.305	93
20.....	128	0.061	0.243	0.305	111
30.....	73	0.035	0.138	0.305	148
40.....	18	0.008	0.033	0.305	300
Uniformly Distributed Tubes					
10.....	183	0.087	...	1.0	165
20.....	128	0.061	...	1.0	197
30.....	73	0.035	...	1.0	260
40.....	18	0.008	...	1.0	545

NOTE.—The network tubes have parameters consistent with the tube models of C98. For explanation of symbols see § 2.1 and Appendix A.

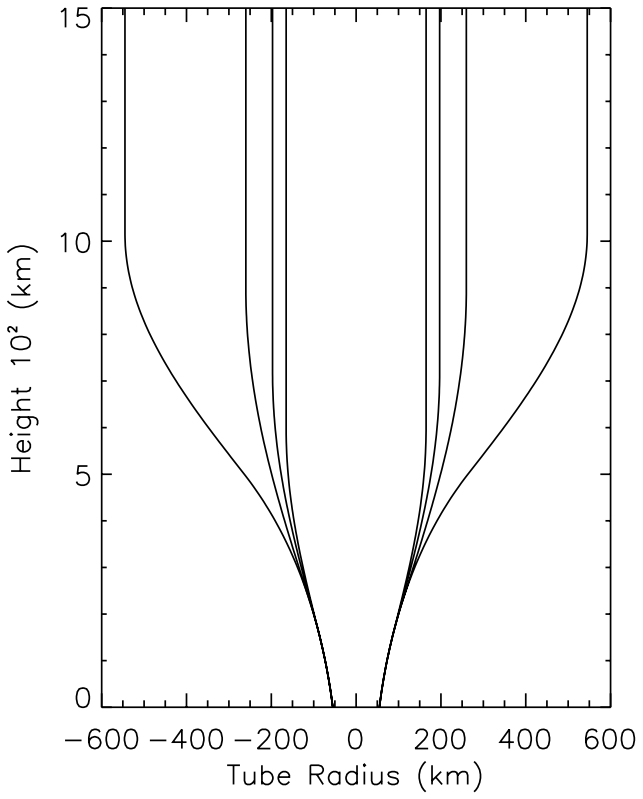

FIG. 1.—Shape of flux tubes. The flux tube parameters correspond to uniformly distributed tubes.

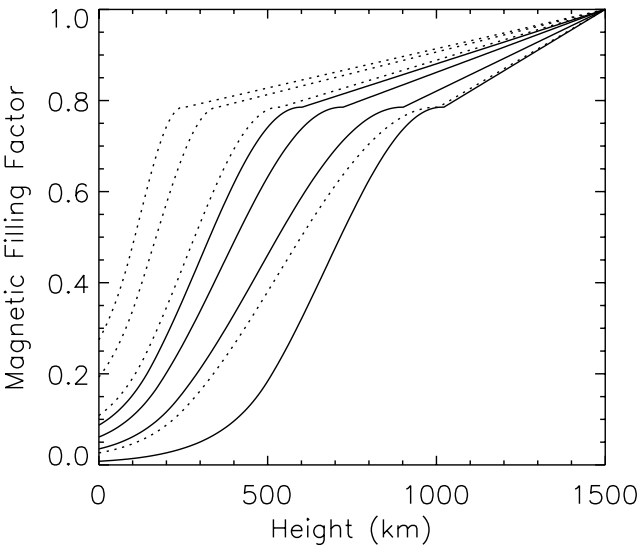

FIG. 2.—Magnetic filling factors for uniformly distributed tubes (*solid lines*) and network tubes (*dotted lines*) as function of height. For the network tubes, the filling factors are for the network area only. The cases shown are those for $P_{rot} = 10, 20, 30, 40$ days, respectively.

In the case of magnetic flux tubes being arranged in a chromospheric network, the chromospheric magnetic filling factor is well below unity, implying that the photospheric flux tube distribution must be explicitly prescribed. We assume that the chromosphere consists of block units of length L with strips of width a representing the chromospheric network. The total magnetic area is thus given by

$$F_S = 2aL - a^2 .$$

With f_S being the photospheric magnetic filling factor within the strip and f_0 being the (average) photospheric filling factor, we find

$$f_S(2aL - a^2) = f_0 L^2 .$$

Note that f_S is related to $f_N = 4f_0$ (see C98) and is defined as $f_S = (\pi/4) f_N$ (see Table 1). The discrepancy between f_S and f_N is solely due to the difference between quadratic and circular tube expansion at the height of the tube merging. The width of the strip a is given by $a = 2r_\infty$, where r_∞ is the top opening radius of the tubes (see Appendix A). The number of flux tubes N per strip of a block unit (i.e., chromospheric network region) is given by $N = L/a$. With f_0 and f_S as free parameters, N is given by

$$N = (f_S/f_0)(1 + \sqrt{1 - f_0/f_S}) .$$

However, it is more convenient to select the *average* chromospheric filling factor f_C rather than f_S as free parameter to describe the number of flux tubes in a block unit of the chromospheric network. In the case of flux tubes uniformly distributed on the stellar surface, we always have $f_C = 1.0$. In the case of flux tubes arranged as a chromospheric network, the number of tubes per strip depends on f_C. The relation between f_C and N is given by

$$f_C = (2N - 1)a^2/L^2 = 2/N - 1/N^2 .$$

In our model, we intend to have $f_C \simeq 0.30$, which would give 6.12 flux tubes per strip. As we want to use $N = 6$ instead, the resulting average chromospheric filling factor is $f_C = 0.305$. Thus, the described approach allows us to construct generalized inhomogeneous flux tubes distributions with flux tubes being arranged as a chromospheric network.

2.2. (*Magneto-*)*Acoustic Energy Generation and Wave Propagation*

One of the main goals of this paper is to calculate the efficiency of heating of the nonmagnetic and magnetic components of stellar chromospheres. To perform these calculations, it is necessary to know the initial wave energy fluxes carried by acoustic and longitudinal tube waves, and their periods, which we obtain using the recent results of Ulmschneider, Theurer, & Musielak (1996) and Ulmschneider & Musielak (1998), respectively.

Acoustic wave energy spectra and fluxes for stars of different spectral types and different luminosities have been computed by Ulmschneider et al. (1996), who used the Lighthill-Stein theory of sound generation with modifications described by Musielak et al. (1994). These modifications included an improved description of the spatial and temporal parts of the turbulent energy spectrum in stellar convection zones. The turbulence has been described by using an extended Kolmogorov energy spectrum and a modified Gaussian frequency factor (the eKmG-spectrum). There is only one free parameter in these calculations, namely, the mixing-length parameter $\alpha_{\rm ML}$, which is in the range between 1.0 and 2.5 depending on the hydrodynamic and thermodynamic structure of the convective flow (e.g., Cattaneo et al. 1991; Rast & Toomre 1993, and references therein). One way of constraining $\alpha_{\rm ML}$ is to evaluate up-to-date stellar convection models for specific stars. Nordlund & Dravins (1990) presented sophisticated time-dependent convective models based on three-dimensional hydrodynamics and three-dimensional nongray radiative transfer for a set of main-sequence stars and subgiants. Based on a set of models, which also included a K1 V star, they argued that $\alpha_{\rm ML}$ might be $\simeq 1.5$ (or somewhat larger). This value is adopted here, which according to Ulmschneider et al. (1996) yields an initial acoustic wave energy flux of $F_M = 8.0 \times 10^6$ ergs cm^{-2} s^{-1} for our target stars. Using the acoustic wave energy spectra presented by the same authors, we find that the maximum amount of energy is carried by acoustic waves with period $P_{w,\rm ac} = 60$ s. These values are therefore used in our acoustic wave calculations.

In recent computations for the generation of longitudinal tube waves in the solar atmosphere (Ulmschneider & Musielak 1998), the nonlinear time-dependent response of a thin vertical flux tube to the external pressure fluctuations is numerically simulated. The same method has been adopted by Ulmschneider, Musielak, & Fawzy (1999) to calculate the fluxes and spectra for longitudinal tube waves propagating in stellar atmospheres. These numerical fluxes are an order of magnitude larger than those calculated using analytical methods (Musielak et al. 1995). Taking the mixing-length parameter $\alpha_{\rm ML} = 1.5$ and using the results given by Ulmschneider et al. (1998), we find that the energy flux carried by longitudinal waves in atmospheres of K2 V stars is $F_M = 1.2 \times 10^8$ ergs cm^{-2} s^{-1} largely independent of the tube shapes. For $\alpha_{\rm ML} = 2.0$, we would obtain $F_M = 1.8 \times 10^8$ ergs cm^{-2} s^{-1}. The maximum energy is carried by longitudinal tube waves that have periods close to 60 s. We thus take $P_{w,m} = 60$ s in our calculations. Now, we must consider that the interaction between magnetic flux tubes and the external turbulent motions leads not only to the generation of longitudinal tube waves but also to transverse tube waves. As shown by Huang, Musielak, & Ulmschneider (1995), the efficiency of generation of these waves can be 1 order of magnitude higher than the longitudinal waves. On the other hand, only a small fraction of this energy is directly transferred to longitudinal waves as a result of nonlinear mode coupling (Ulmschneider et al. 1991). It is also known that the energy carried by transverse tube waves leaks efficiently to the external medium and that acoustic waves present in the external medium promote the excitation of longitudinal tube waves (Huang, Musielak, & Ulmschneider 1999). Obviously, taking all these processes into account is outside the scope of this paper. However, we still must account for some of this extra energy available for the heating. Hence, we correct the above-given initial wave energy flux by adding to it a small fraction of the energy carried by transverse tube waves. Writing $F_M = F_{\rm LTW} + \eta F_{\rm TRW}$ and taking $F_{\rm LTW} = 1.2 \times 10^8$ ergs cm^{-2} s^{-1}, $F_{\rm TRW} = 1.0 \times 10^9$ ergs cm^{-2} s^{-1}, and $\eta = 0.1$, we obtain $F_M = 2.2 \times 10^8$ ergs cm^{-2} s^{-1}. This value is adopted for our calculations.

The computed initial wave energy fluxes and wave periods can now be used to compute the models of acoustically and magnetically heated components of stellar chromospheres. The method for calculating the acoustically

heated component is identical to that used by B98. We utilize the modified method of characteristics, as described in our previous papers (Ulmschneider et al. 1977, 1978; Schmitz, Ulmschneider, & Kalkofen 1985; Ulmschneider, Muchmore, & Kalkofen 1987; Rammacher & Ulmschneider 1992) to solve the one-dimensional hydrodynamic equations consisting of the continuity, momentum, and energy equations. At the bottom of the atmosphere at optical depth $\tau_{5000} = 1$, we introduce sinusoidal acoustic waves with periods of 60 s and amplitudes determined by the adopted initial wave energy flux. The propagation of these waves is simulated numerically to the point of shock formation and beyond. The shocks are treated as discontinuities by solving the Rankine-Hugoniot equations for acoustic waves and are permitted to grow to arbitrary strength. At the top of the atmosphere we use a transmitting boundary condition following Ulmschneider (1986). Radiative losses (and gains) due to the H^- continuum and the Mg II k line are computed by solving the corresponding radiative transfer equations. This treatment requires additional explanation as in reality there are many chromospheric lines (the Ca II H and K lines, the Ca II infrared triplet, the Mg II h and k lines, and Fe II lines—just to mention the most prominent ones) that contribute significantly to the total radiative losses from stellar chromospheres; note that these lines have to be calculated by solving radiative transfer equations with partial redistribution (PRD) assuming multilevel atoms. The inclusion of all these lines is, however, beyond the scope of the present paper. Thus, our approach is to compute only the Mg II k line, but with the complete redistribution (CRD) and scale this line up to represent the total chromospheric losses; note that we could have taken either the Mg II h line or one of the Ca II lines and obtain virtually the same result by appropriate scaling. The radiative transfer equations considered here are solved together with the statistical equilibrium equations for NLTE populations. Compared to earlier work, we also consider various technical improvements, including the treatment of NLTE ionization for the included chromospheric emitters (Rammacher & Cuntz 1991), and the use of the revised operator splitting method for the Mg II k line (Buchholz et al. 1994) with the proper inclusion of the shocks; similar improvements are adopted in our calculation of the Ca II emission lines (see § 2.3). Now, when the full balance is established between the locally dissipated acoustic wave energy and the local radiative losses, new values of atmospheric temperature and density are calculated. This gives the time-dependent model for the acoustically heated component of stellar chromospheres.

To calculate the propagation and dissipation of longitudinal tube waves, we use our previous treatment of these waves in the solar atmosphere (e.g., Herbold et al. 1985; Rammacher & Ulmschneider 1989; Fawzy et al. 1998). The set of nonlinear MHD equations is simplified by taking into account the so-called thin flux tube approximation and is solved by using the modified method of characteristics (see Appendix B). The waves are nonlinear and radiatively damped. A thin, vertically oriented magnetic tube is embedded in a magnetic-free medium, and the initial wave energy flux is imposed on the tube at the atmospheric height corresponding to the optical depth $\tau_{5000} = 1$. The propagation of longitudinal waves with periods of 60 s is investigated by performing time-dependent numerical simulations. The waves introduced by an oscillating piston at the bottom of the flux tubes are again followed to the point of shock formation and beyond. To reduce the effect of large-scale oscillations during the switch-on phase of the wave, the initial wave energy flux is gradually increased over a time span of 10 wave periods in all models presented. The atmospheric height of the initially undisturbed tube models extends originally up to 1500 km (corresponding to 16.2 pressure scale heights H_p) but may increase during the course of the wave computation due to the mechanical heating and wave pressure. The energy dissipation by the shocks is calculated self-consistently by solving the MHD Rankine-Hugoniot relations that also consider the distensibility of the tubes (Herbold et al. 1985). The wave energy dissipated by these shocks is balanced against the radiative losses, which are treated in the same way as described above for the acoustically heated models. Again, when the full balance between the locally dissipated magnetic wave energy and the local radiative losses is established, new values of atmospheric temperature and density are calculated. This gives the time-dependent model for the magnetically heated component of stellar chromospheres. Note that the computed model strongly depends on the adopted shape of the flux tube.

2.3. *Emission-Line Simulation by Multiray Radiative Transfer*

In order to compute the chromospheric emission in a given line from our theoretical models, several different effects need to be considered. It is known that the chromospheric emission depends on the total number of tubes, the voids between the tubes ("canopies"), the distribution of the tubes, and radiative transfer effects. Intriguing examples of radiative transfer for the Ca II K line along multiple rays (1.5-dimensional) based on PRD passing through two-dimensional magneto*static* models for the quiet solar chromosphere have already been given by Solanki, Steiner, & Uitenbroeck (1991), which could reproduce a variety of observational features including the spatially averaged Ca II K line profile. Earlier results for the Sun for regions of high and low magnetic filling factors were given by Rammacher & Ulmschneider (1989) who also used a multiray 1.5-dimensional radiative transfer method that was, however, based on CRD. Their results show that the emission in Mg II and Ca II is considerably enhanced in models with higher magnetic filling factors. The effect of different shapes of the flux tubes on the chromospheric emission has recently been investigated by Fawzy et al. (1998).

As mentioned before (see § 2.1), we consider two different flux tube distributions: uniformly distributed tubes and tubes arranged in strips to simulate a chromospheric network. The basic element of both distributions is the so-called tube row: a strip of expanding tubes with identical geometries at all heights (see Fig. 3). For the tubes, we assume that their thermodynamic structure is well determined by the theoretical models (see § 3.1). For the simulation of the Ca II emission lines, we assume that each tube is filled with a different wave phase (selected from a total of four) from our MHD wave models. Therefore, we effectively ensure that the line fluxes and profiles represent a mixture of the different wave phases existing in the K2 V star chromosphere. The total number of tubes $\hat{N}$ in a row used for the radiative line simulation depends on the angle between the surface normal and the line of sight; for large angles, more tubes are intersected by the ray path. With H being the height of the atmosphere and r_0 the bottom tube

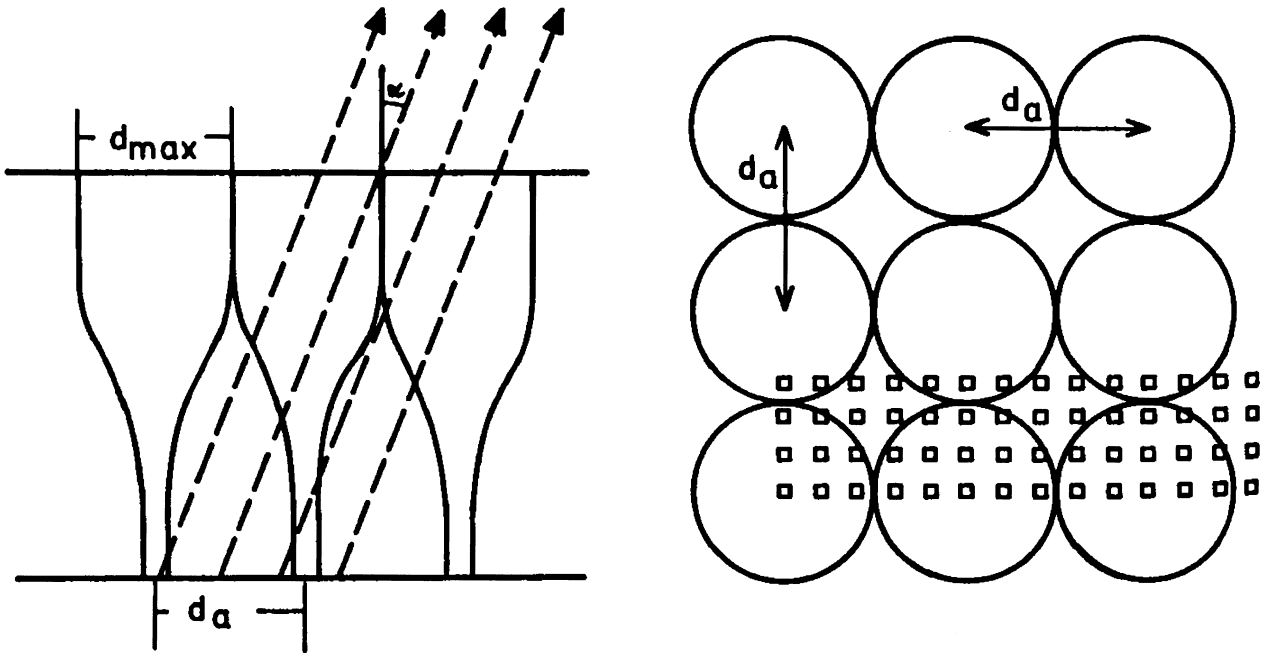

FIG. 3.—Array of flux tubes as used for calculating the radiative transfer. Given are the views from the side (*left*) and from the top (*right*). In our models we consider rays of five different angles.

radius, we have

$$\hat{N} = H \tan\alpha \sqrt{f/(\pi r_0^2)} + 5 .$$

The external atmosphere is filled with the properly chosen phase of the acoustic wave calculation (see § 2.2). For simplicity we do not average over different wave phases for calculating the Ca II emission flux of the external atmosphere. Therefore, we select a wave phase that closely resembles the Ca II H + K emission obtained by B98 for pure acoustic heating. The acoustic heating model refers to the situation with no magnetic flux tubes existing.

The tubes are assumed to spread with height, eventually reaching the tube top opening radius r_∞, where the tubes start to merge. Above this height, the remaining space between the tubes is gradually filled with magnetic fields so that the filling factor approaches 100% at the top of the atmospheric model, which is at $z = 1500$ km. The stellar surface elements are sampled equidistantly every 40 km for a total of 600 spatial grid points. The radiative transfer is then calculated along different rays which, for a given angle α, contribute to the integrated line profile (see Fig. 3). Because of the complex tube geometry, the intensity profiles vary strongly for different angles; therefore, it is mandatory to use more than one angle for the radiative transport. Here, we use five angles for our calculations ($\cos\alpha = \mu = 0.9$, 0.7, 0.5, 0.3, and 0.1), which represent five annuli of identical surface area. This ensures that all surface areas of our chromospheric models equally contribute to the integrated line flux. Note that the given values of μ are closely related to the zero points of the Legendre polynomials (see Rammacher, Ulmschneider, & Cuntz 1999 for details).

The radiative transfer for the Ca II K line is computed with partial redistribution and by using a two-level atom. To perform these calculations, we utilize the modified operator splitting method as described by Ulmschneider (1994). The redistribution is computed using the R II function of Gouttebroze (1986) with the data of the respective atomic model. We use 47 frequency points, distributed within ± 10 Å of line center. Most of these points are concentrated within ± 0.3 Å of line center since the K_1 minima in the models are always located in this range. This interval is also used to calculate the emitted flux.

3. RESULTS AND DISCUSSION

3.1. *Magnetic and Acoustic Heating Models*

In order to construct two-component, theoretical chromosphere models, it is necessary to calculate time-dependent models for both acoustic and magnetic chromospheric components. In this work, we compute these models separately, which implies that no mutual interaction between the components is considered. For the computation of the emergent Ca II H + K flux, however, both components are combined, and the Ca II line fluxes and profiles are calculated using our multicomponent radiative transfer method (see § 2.3). Magnetic component models of this type have already been described in detail by C98, along with their deduced MHD properties. The r_∞ values of the tubes (see Table 1) adopted in that paper had been selected in accordance to the chromospheric network tube distribution, i.e., $f_N = 4f_0$, although it was erroneously stated there that the tubes were uniformly distributed on the stellar surface. The physical properties of the tubes clearly depend on the shape of the tubes and the initial wave properties, but they are not *directly* dependent on the photospheric flux tube distribution. Consequently, the flux tube calculations by C98 are fully relevant to this paper.

Given the results of C98, we thus can focus solely on the MHD properties of those models with flux tubes that are uniformly distributed over the stellar surface (see Table 1 for r_∞ values). Figures 4 and 5 give snapshots of tube models for stars with $P_{\rm rot} = 10$ and 40 days, respectively. Figure 6 shows a snapshot of the acoustic heating model for the nonmagnetic surface region. As r_∞ for the second star is much larger, the magnetic field strength within the tubes becomes much more reduced. The magnetic field strength at the top of the tubes in the second star is only 21 G com-

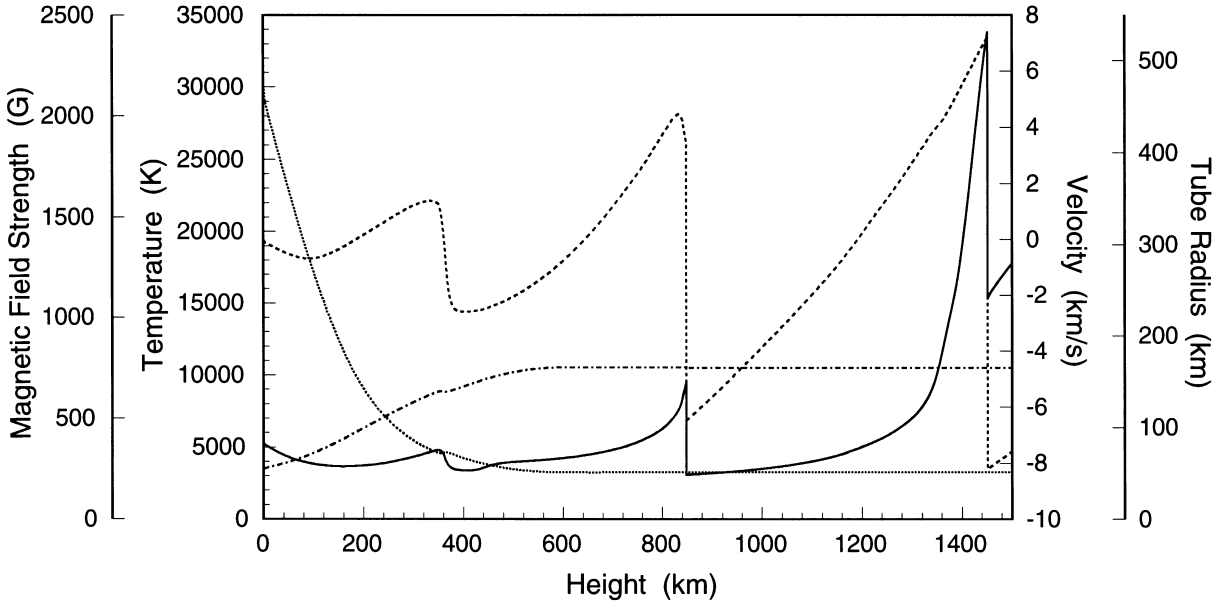

FIG. 4.—Snapshot showing a MHD flux tube model for K2 V stars with rotation periods of $P_{\rm rot} = 10$ days. The distribution of flux tubes is assumed as being uniform over the stellar surface. The figure depicts the velocity (*dashed line*), the temperature (*solid line*), the magnetic field strength (*dotted line*), and the shape of the tube (*dashed-dotted line*) as function of height. The elapsed time of the wave is $t = 1229$ s.

pared to 233 G in the first star because of magnetic flux conservation. At the bottom of the tubes we have $B_0 = 2100$ G in both stars (see § 2.1). The reduced spreading of the tubes in the faster rotating star leads to a smaller dilution of the magnetic wave energy flux, which reduces the atmospheric temperatures particularly behind the shocks (see below).

The density structure of the acoustic and magnetic heating models for $P_{\rm rot} = 10$ and 40 days is given in Figure 7, which shows that the time-averaged density is notably lower in the magnetic heating models owing to the magnetic contribution to the horizontal pressure balance. At the bottom of the tube the gas pressure inside and outside the tube (p_i and p_e, respectively) is $p_i : p_e = 1:4$ in agreement with our assumption (see § 2.1). At larger atmospheric heights, the decrease of density in the model with $P_{\rm rot} = 10$ days is significantly moderated owing to atmospheric heating and wave pressure. Figure 8 shows the wave energy flux for the acoustically and magnetically heated models calculated for stars with $P_{\rm rot} = 10$ and 40 days. In all these models, the decrease of the wave energy flux with height is influenced by the wave energy dissipation as well as by the radiative energy losses, which are particularly important at chromospheric heights. In the two magnetically heated models, the geometrical dilution of the wave energy flux at heights beyond 300 km is also a major effect, especially in the model with $P_{\rm rot} = 40$ days.

The snapshots shown in Figures 4 and 5 refer to time instants after 20 wave periods. The model for $P_{\rm rot} = 10$ days contains two shocks, which are at heights $x_{\rm sh} = 848$ and

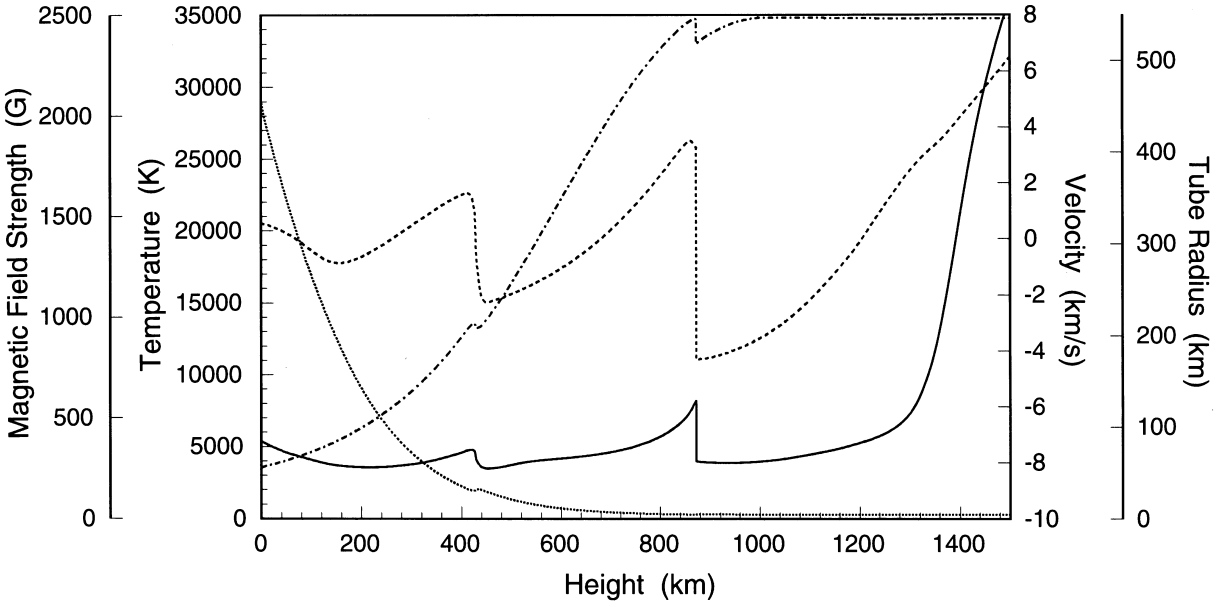

FIG. 5.—Same as Fig. 4, but now for a star with a rotation period $P_{\rm rot} = 40$ days. The elapsed time of the wave is $t = 1242$ s.

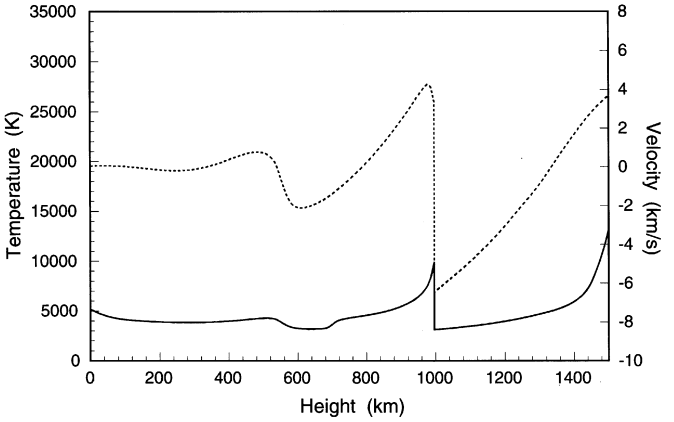

FIG. 6.—Similar to Fig. 4, but now for the acoustic wave model for the outer tube region. The elapsed time of the wave is 1245 s.

1451 km and have shock strengths of $M_{sh} = 2.68$ and 2.09, respectively. The outer shock is located within a part of the atmosphere where Ca II is completely ionized because of the postshock temperature $T^{(2)} \gtrsim 30{,}000$ K. This temperature is consistent with the temperature range of solar-type transition regions. In the postshock region of the inner shock, the relative number density $q(\text{Ca II}) = n(\text{Ca II})/n(\text{Ca})$ (where n is the number density) is moderately large, indicating the importance of the Ca II emission for the energy balance in flux tubes. For the longitudinal tube waves considered here, we find that the shock strength increases steadily with height in the lower and middle part of the atmosphere inside the tubes. Beyond a height of $\simeq 1200$ km, however, M_{sh} in the tube model with $P_{rot} = 10$ days decreases, which is merely a consequence of the geometrical dilution of the wave energy flux owing to the increase of the tube spreading with height. Other effects which lead to a change of M_{sh} with height include the energy dissipation by the shocks and the radiative energy losses in the postshock regions. The evolution of shock strengths as a function of height for

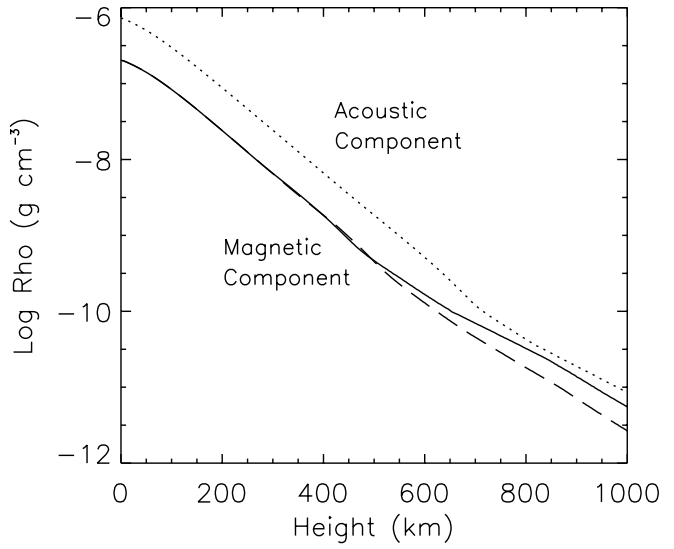

FIG. 7.—Time-averaged densities for the acoustic and magnetic component as function of height. The figure depicts the acoustic heating model (*dotted line*) and the MHD tube models for $P_{rot} = 10$ days (*solid line*) and 40 days (*dashed line*) while assuming uniformly distributed flux tubes. Time-averaging has been performed over a time span of 120 s, i.e., two wave periods.

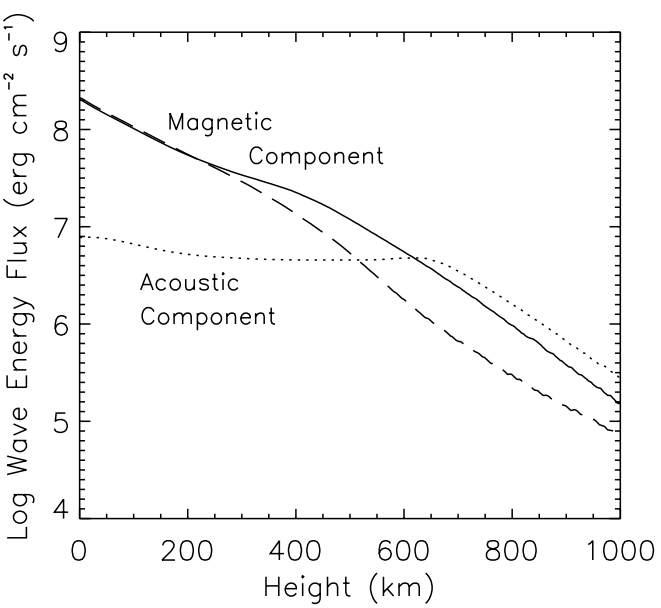

FIG. 8.—Time-averaged wave energy fluxes for the acoustic and magnetic component as function of height. The figure depicts the acoustic heating model (*dotted line*) and the MHD tube models for $P_{rot} = 10$ days (*solid line*) and 40 days (*dashed line*) while assuming uniformly distributed flux tubes. Time-averaging has been performed over a time span of 360 s, i.e., six wave periods.

the wave model $P_{rot} = 10$ days is depicted in Table 2, which gives the shock wave parameters [M_{sh}, x_{sh}, $q(\text{Ca II})^{(2)}$, and $T^{(2)}$] for four consecutive wave phases at 15 s time intervals.

Figure 5 presents a snapshot of a wave for a star with $P_{rot} = 40$ days after the insertion of 20 wave periods. Here we find the presence of strong expansion beyond 1200 km of height as already seen in the model with $P_{rot} = 10$ days. The model $P_{rot} = 40$ days also shows a shock at height $x_{sh} = 872$ km with a shock strength of $M_{sh} = 1.95$. Note that x_{sh} in the models with $P_{rot} = 10$ and 40 days are very similar: in the former model, we have $x_{sh} \simeq 370$ km, whereas in the latter model this height is shifted somewhat beyond 400 km with the exact value depending on the elapsed time of the wave. This result is similar to the case of network tubes discussed by C98 who found that in the star with $P_{rot} = 10$ days, the shock formation occurs at 371 km (i.e., $4.4H_p$), whereas in the star with $P_{rot} = 40$ days, $x_{sh} = 435$ km (i.e., 5.0 H_p). These results mirror the similarities of the tube spreading functions at x_{sh} in the two types of models calcu-

TABLE 2

PHASE DEPENDENCE OF F_{HK} AND SHOCK WAVE PARAMETERS

Phase	log F_{HK} (cgs)	M_{sh}	x_{sh} (km)	$T^{(2)}$ (K)	$q(\text{Ca II})^{(2)}$
1	5.83	2.68	848	9510	0.28
		2.09	1453	33,550	0.00
2	5.91	1.70	464	7050	0.92
		2.76	978	10,190	0.15
3	6.15	2.09	580	7830	0.71
		2.79	1119	11,210	0.06
4	6.05	2.49	703	8730	0.49
		2.71	1282	12,730	0.02

NOTE.—The time difference between two consecutive phases is 15 s, and the elapsed time of phase 1 is 1.23×10^3 s. The model refers to uniformly distributed flux tubes for the star $P_{rot} = 10$ days.

lated. It should be noted, however, that at $x_{sh} \gtrsim 800$ km, the shock strengths are significantly different in models with $P_{rot} = 10$ and 40 days (see Figs. 4 and 5 and Table 2). This result is due to the increased spreading of the tubes in stars with slower rotation rates. Because of this property, the wave energy flux is distributed over an increasingly greater cross section area, which decreases the waves amplitudes, M_{sh}, $T^{(2)}$, and the energy dissipation rates of the waves (see C98). The geometrical dilution of the wave energy flux is also relevant for the emergent Ca II emission (see § 3.2).

To calculate the emerging Ca II emission flux, we must also take into account the areas between the tubes. Therefore, we computed a time-dependent acoustic heating model. Figure 6 depicts a snapshot found after 1245 s, which is again after the insertion of 20 wave periods. The shock strength in the acoustic wave model is $M_{sh} = 2.62$. The shock strength is essentially independent of the atmospheric height owing to the fact that we considered monochromatic waves; for analytic expressions of the limiting shock strength, see Ulmschneider (1970) and B98. The mean temperature in the acoustic heating model at 800 km (which is in the upper part of the Ca II line formation region) is 4400 K, similar to the two MHD flux tube models with $P_{rot} = 10$ and 40 days previously discussed. The acoustic heating model also shows that the energy dissipation rate for the shocks is intermediate between the MHD wave models of $P_{rot} = 10$ days and $P_{rot} = 40$ days. As discussed in § 4, the acoustic wave model turns out to be pivotal for properly representing the chromospheric emission in the absence of flux tubes. We find that when the nonmagnetic regions dominate, the chromospheric emission agrees with the basal flux emission as found in inactive stars (e.g., Rutten et al. 1991; Schrijver 1995) and theoretically described by B98.

3.2. *Results from* Ca II *Line Simulations*

The most important goal of this paper is to simulate the chromospheric emission for our two-component chromosphere models. Contrary to C98, where the line emission was estimated from the local cooling rates of the flux tubes, we now simulate the chromospheric emission using detailed radiative transfer in a two-component chromospheric structure with arrays of flux tubes. Figure 9 represents the Ca II K line profiles for different angles for the model with $P_{rot} =$ 10 and 40 days, respectively. Here we see that the line emission is strongest in the case when the flux tubes are viewed at small μ (i.e., large angles α). In this case, the rays intersect a considerably large number of flux tubes, which means that there is a high contribution of magnetically heated regions to the total emission. As expected, this emission is strongest for narrow tubes related to fast rotating stars largely owing to the relatively small voids between the tubes. Figure 9 shows the results for the case of uniformly distributed tubes. It is found that the Ca II K line emission is about a factor of 6 greater in the case of $P_{rot} = 10$ days than for $P_{rot} = 40$ days.

Because of our two-level atom approach, we have calculated the line transfer for the Ca II K line only. However, for comparison to observations we are interested in the total Ca II H + K line flux, referred to as F_{HK}. In earlier papers (e.g., B98), that value has been obtained by doubling the line flux of Ca II K, which is a valid approximation for low-activity stars. Actually, the Ca II H flux is reduced relative to the Ca II K flux in more active stars (Vaughan, Preston, &

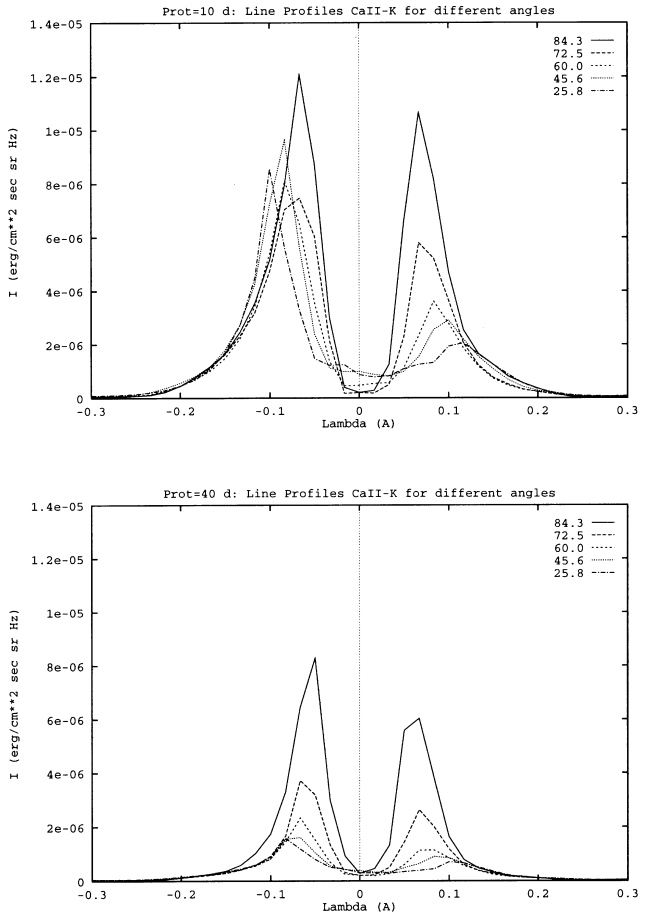

FIG. 9.—Ca II K line profiles for different angles for the model with $P_{rot} = 10$ days (*upper figure*) and 40 days (*lower figure*).

Wilson 1978). To account for this, we compute a scaling factor $R_{K/H}$ depending on the stellar activity which is calibrated in terms of P_{rot} (see § 4.1). This scaling factor can be utilized to calculate the total F_{HK} for our theoretical models. Based on this relationship we find that the Ca II K flux must be multiplied by a factor of 1.87, 1.89, 1.92, and 1.95 for stars with $P_{rot} = 10$, 20, 30, and 40 days, respectively. Table 3 depicts the dependence of F_{HK} on the flux tube distribution. We find that uniformly distributed flux tubes produce the highest F_{HK} for most stars. The reason is that in those stars the voids (i.e., magnetic canopies) between the tubes are of less importance. The difference in

TABLE 3

DEPENDENCE OF F_{HK} ON THE FLUX TUBE DISTRIBUTION

P_{rot} (s)	log F_{HK} (cgs)	log F_{HK}^{ntw} (cgs)
10.....	6.01	5.83
20.....	5.94	5.78
30.....	5.81	5.74
40.....	5.51	5.58
(Basal).....	5.49	5.49

NOTE.—F_{HK} refers to uniformly distributed tubes and F_{HK}^{ntw} to flux tubes arranges as a chromospheric network. The values for "basal" refer to a pure acoustic heating model.

F_{HK} between the different flux tube distributions considered in this paper is most pronounced in fast rotating stars.

The fact that the Ca II H + K emission is significantly lower in the star with $P_{rot} = 40$ days is fully consistent with the behavior of the wave energy flux as function of atmospheric height (see Fig. 8). Since flux tubes spread more with height on slower rotators, a smaller amount of energy is available in the Ca II formation region. The calculated models show remarkable behavior concerning the efficiency of converting F_M into F_{HK}. Although the initial magnetic wave energy flux is greater by a factor of 27 than the initial acoustic wave energy flux, the F_{HK} emission by the two-component chromosphere models is increased only by a factor of 1.5–4.5 depending on the model. We identify two reasons for this behavior: First, in magnetic flux tubes, the wave energy flux is considerably reduced with atmospheric height due to geometrical dilution. Second, in magnetic flux tubes, the density inside the tubes is significantly lower than outside the tubes, which further reduces the Ca II radiative emission.

We also made a preliminary study of the effects of the wave parameters on the Ca II H + K line intensity. For this study, we focused on the star with $P_{rot} = 10$ days and uniformly distributed tubes. We varied the longitudinal flux tube wave period $P_{w,m}$ between 30 and 90 s, compared with $P_{w,m} = 60$ s used in our standard model. We find that although M_{sh} and thus the mechanical energy dissipation rates increased substantially with increasing $P_{w,m}$, the resulting Ca II was found to be *largely independent* of the wave period adopted. The variation obtained was less than 20%. The reason for this behavior is due to the balancing influence of Ca II–Ca III ionization. Although increased energy dissipation often results in increased radiative emission, it also depletes the Ca II number densities in the line formation region, because high energy dissipation rates favor a high number density of Ca III behind the shocks owing to increased postshock temperature. In another study, we also varied the mechanical wave energy flux. We found some dependence of the emergent Ca II H + K line intensity on F_M. We plan to evaluate this in a separate paper, which will also include a more detailed analysis of the effects and behavior of mode coupling (see § 2.2).

4. COMPARISON WITH OBSERVATIONS

4.1. *The* Ca II *Emission–Stellar Rotation Relationship*

In § 3, we found that owing to the physical properties of the magnetic flux tubes, the heating and chromospheric emission is significantly increased in the magnetic component and is strongest in flux tubes with the small spreading factors, expected on rapid rotators. We calculated the theoretical Ca II H + K emission flux for the cases of uniformly distributed tubes and for the tubes arranged as a chromospheric network. We now want to compare those fluxes with observations. In order to give a comparison with a significant number of stars, we have chosen a set of stars ranging from spectral type K0 V to K3 V with $B-V$ between 0.78 and 0.98. The stars have been taken from the data set by Baliunas et al. (1995). Note that only stars with known rotational periods P_{rot} and reliable Ca II measurements are taken into consideration. Where a range of rotation period detections is available (see Donahue, Saar, & Baliunas 1996), we used the average P_{rot}. Note that $v \sin i$ measurements cannot substitute for P_{rot}, which significantly limits the number of stars that can be considered. As we want to concentrate on single stars, we also disregard binary stars with significant binary interaction, including tidally synchronized binaries. In addition, we did not consider stars with stellar rotation periods smaller than 5 days, which allows us to focus on the linear part (i.e., nonsaturated) of the Ca II emission–stellar rotation relationship. This enables us to provide a detailed statistical analysis both of our observational data and the results from our theoretical models.

The data for the selected stars are given in Table 4. There are two different methods for calibrating the Ca II H+K fluxes introduced by Noyes et al. (1984) and Rutten (1986) (see Appendix C). To make a comparison between our theoretical results and the observations (see Fig. 10), we used the calibration by Noyes et al. (i.e., F'_{HK}). Here we see that our

TABLE 4

STELLAR DATA

HD	Sp. Type	$B-V$	P_{rot} (days)	$\langle S \rangle$	$\langle S \rangle_{min}$	log F_{HK} (cgs)	log F'_{HK} (cgs)	log F'_{HK}(min) (cgs)	$R_{K/H}$
17925.....	K2	0.87	6.8	0.653	...	6.43	6.26	...	...
22049.....	K2 V	0.88	11.7	0.496	...	6.26	6.11	...	...
115404.....	K2 V	0.93	18.5	0.535	...	6.17	6.01	...	1.137
165341A.....	K0 V	0.78	19.7	0.392	...	6.17	6.03	...	1.115
155886.....	K0 V	0.86	20.7	0.375	...	6.14	6.01	...	1.123
155885.....	K1 V	0.86	21.1	0.384	...	6.16	6.02	...	1.105
149661.....	K2 V	0.82	21.1	0.339	...	6.16	6.04	...	1.097
10476.....	K1 V	0.84	35.2	0.196	0.170	5.69	5.69	5.59	1.035
160346.....	dK3	0.96	36.4	0.300	0.215	5.77	5.69	5.52	1.068
4628.....	K2 V	0.88	38.5	0.230	0.195	5.76	5.71	5.62	1.087
166620.....	K2 V	0.87	42.4	0.190	0.165	5.60	5.62	5.53	1.013
219834B.....	K2 V	0.88	43.0	0.204	0.180	5.59	5.59	5.52	...
3651.....	K0 V	0.85	44.0	0.176	0.155	5.54	5.60	5.51	1.031
16160.....	K3 V	0.98	48.0	0.226	0.195	5.50	5.51	5.44	...

NOTE.—$\langle S \rangle$ is the Ca II H + K flux index, and $\langle S \rangle_{min}$ is the value corresponding to the minimum activity phases of the stars (both from Baliunas et al. 1995). P_{rot} is the *average* value of the rotation period from Donahue et al. 1996 or Baliunas et al. 1996, otherwise from Rutten 1986. F_{HK} and F'_{HK} are based on the Rutten et al. 1991 and Noyes et al. 1984 calibrations, respectively; F'_{HK}(min) is computed from $\langle S \rangle_{min}$. $R_{K/H} = F'_K/F'_H$ is derived from S_H and S_K in Vaughan et al. 1978. The stellar spectral types and $B-V$ are from Hoffleit & Jascheck 1982.

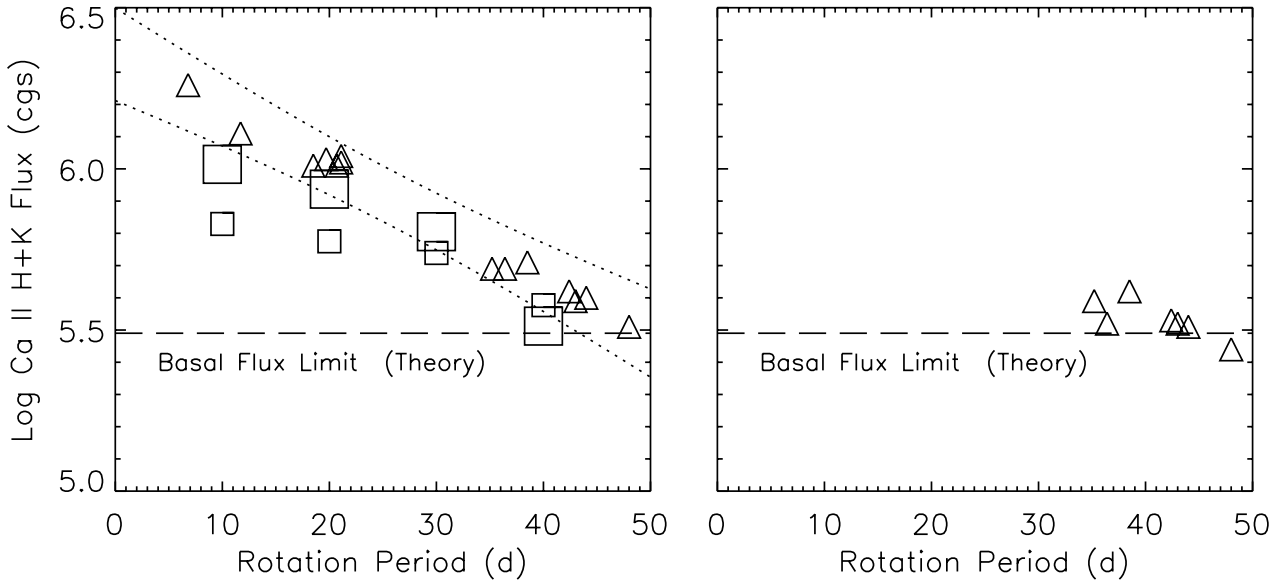

FIG. 10.—*Left:* Ca II H + K emission flux (log units; cgs) as function of stellar rotation. The triangles give the observational results for a set of stars with spectral type between K0 V and K3 V (see Table 4). The squares indicate the results from two-component theoretical chromosphere models (magnetic and acoustic heating; see text) for K2 V stars of different rotation periods. Large squares refer to models with uniformly distributed flux tubes, small squares to models with flux tubes arranged as chromospheric network regions. The dotted lines indicate the 3 σ flux limits permissible by the observations. Here only the K2 V stars have been considered. The dashed line indicates the theoretical Ca II H+K basal flux limit given by pure acoustic heating (see B98). *Right:* Ca II H + K emission flux (log units; cgs) as function of stellar rotation for a selected number of stars for which a minimum activity level has been identified based on long-term monitoring. Here the Ca II H+K flux has been recalculated using $S_{\rm min}$.

theoretical results for the models with uniformly distributed flux tubes nicely agree with the observations considering a 3 σ standard deviation for the best fit. As underlying function for the best fit, we assume a linear relationship given by

$$\log F_{\rm HK} = A_{\rm HK} + B_{\rm HK} P_{\rm rot}$$

with $A_{\rm HK}$ and $B_{\rm HK}$ being constants. For calculating the 3 σ standard deviation strip, we consider a mean 1 σ statistical error for $F_{\rm HK}$ of ± 0.035 in the logarithm and a mean 1 σ statistical error for the $P_{\rm rot}$ of ± 1 day (see Soon, Baliunas, & Zhang 1994; Baliunas et al. 1996). As systematic error of the calibration of $F_{\rm HK}$, we assume a value of ± 0.02 in the logarithm. Our statistical method is described by, e.g., Montgomery & Peck (1992).

We note that the agreement between the theoretical results and the observations is highly satisfactory. For stars with $P \gtrsim 25$ days, no significant difference between the two different types of photospheric flux tubes distributions could be identified. For stars with $P \lesssim 25$ days, the best agreement is obtained if it is assumed that the flux tubes are uniformly distributed over the stellar surface. On the other hand, it could still be possible that those stars have higher magnetic energy dissipation owing to enhanced mode coupling between the transverse waves and the longitudinal flux tube waves not considered in our models; this would offset the reduction of the emergent Ca II H + K flux due to the nonmagnetic surface regions. In addition, many magnetically active stars may also be subjected to flare heating. Table 5 gives the summary of the statistical fitting parameters for the different cases considered in this paper. There are no significant changes in $A_{\rm HK}$ and $B_{\rm HK}$ if we consider only K2 V stars (see Table 4 and Fig. 10).

Table 4 also gives information about the observed K/H flux ratios $R_{\rm K/H} = F'_{\rm K}/F'_{\rm H}$ of our target stars. Statistically, this ratio is larger for more active stars (i.e., high $F'_{\rm HK}$ and low $P_{\rm rot}$) than for inactive stars, for which it approaches unity (e.g., for HD 166620 with $P_{\rm rot} = 42.4$ days, $F'_{\rm H}$ is only 2% less than $F'_{\rm K}$). Therefore, we can calculate a $R_{\rm K/H}$-$P_{\rm rot}$ relationship given by

$$R_{\rm K/H} = C_1 + C_2 P_{\rm rot}$$

with $C_1 = 1.19$ and $C_2 = -0.0036$. The values of C_1 and C_2 are largely independent of the fact whether we consider all stars in Table 4 or only the K2 V stars. This relationship can be utilized to scale the calculate Ca II K emission flux toward the total Ca II H + K emission in our theoretical models (see § 3.2).

4.2. *The* Ca II *Basal Flux Emission*

All stars studied in this paper show to some degree variable S values (see Baliunas et al. 1995). Thus $F'_{\rm HK}$ derived from their long-term average $\langle S \rangle$ values include contributions from a variable magnetic dynamo, which likely generates changes in the photospheric $f_0 B_0$ values (e.g., Saar & Baliunas 1992). The only situation in which a purely acoustically heated chromosphere might dominate would be at the magnetic cycle minima of the least active of these stars.

TABLE 5

STATISTICAL FITTING PARAMETERS FOR THE $F_{\rm HK}$-$P_{\rm rot}$ RELATION

Parameter	$A_{\rm HK}$	$B_{\rm HK}(\times 10^{-2})$
Uniform Model.....	6.23 ± 0.10	-1.64 ± 0.35
Network Model	5.93 ± 0.05	-0.79 ± 0.20
Observations: K2 V	6.36 ± 0.03	-1.73 ± 0.10
Observations: K0–K3 V.....	6.37 ± 0.02	-1.79 ± 0.06

NOTE.—The uncertainties of the deduced fitting parameters are 1 σ error bars and do not consider the intrinsic uncertainties of $P_{\rm rot}$ and $F_{\rm HK}$.

Therefore, we have estimated the minimum seasonal average $\langle S \rangle_{\rm min}$ from the plots in Baliunas et al. (1995) for the seven lowest Ca II activity stars of our sample (Table 4) and converted them to $F'_{\rm HK}$(min). Figure 10 gives the comparison of these fluxes to the theoretical Ca II H + K basal flux limit for pure acoustic heating as obtained by B98. The observational results show good agreement with the theoretical models, which strongly supports the conjecture that inactive chromospheres of late-type stars are predominantly heated by acoustic waves.

We caution that even in these cases, there is still likely magnetic activity remaining from both residual dynamo activity at cycle minimum and from a background, nonvariable turbulent dynamo (e.g., Saar 1998; Schrijver et al. 1998). This magnetic dynamo activity is expected also to provide magnetic heating, which may or may not be relevant for the formation of the Ca II H and K lines. Although our present study does not provide evidence of such relevance, further studies are needed. $F'_{\rm HK}$(min) is a good empirical estimate of $F_{\rm ac}$ only if magnetic activity at cycle minimum does not seriously affect Ca II H and K line formation. The presence of magnetic heating itself in low-activity stars is implied by the presence of coronae (e.g., Schmitt 1997), which can barely be heated acoustically (Stępień & Ulmschneider 1989). If magnetic contributions to $F'_{\rm HK}$(min) exist (e.g., Durney, de Young, & Roxburgh 1993; Saar 1998), the model acoustic fluxes should show $F_{\rm ac} < F'_{\rm HK}$(min) even for very inactive stars.

Another topic open for debate is the location of the theoretical basal flux limit itself given by acoustic energy dissipation. B98 presented acoustically heated chromosphere models for stars between F0 V and M0 V and found agreement within a factor of 2 between the theoretical results and the observations over nearly 2 orders of magnitude in emission flux. The result by B98 in the case of K2 V stars is shown for comparison in Figure 10. The theoretical basal flux limits given by acoustic wave computations should be a topic of future research as many important effects were omitted in the models, including (1) using acoustic frequency spectra instead of monochromatic waves (Fleck & Schmitz 1993; Sutmann & Ulmschneider 1995; Theurer 1998), (2) inclusion of thermal bifurcation due to CO molecules (Cuntz & Muchmore 1994), and (3) time-dependent (i.e., noninstantaneous) ionization of hydrogen (Carlsson & Stein 1992; Cuntz & Höflich 1999). These effects are expected to affect the theoretical Ca II H + K basal flux limits suggesting the necessity of future investigations.

5. CONCLUSIONS AND OUTLOOK

We computed time-dependent two-component (acoustic and MHD) chromospheric models for K2 V stars with different levels of magnetic activity. The heating of the nonmagnetic component is determined by the acoustic energy dissipation, whereas the heating of the magnetic component is determined by the energy dissipation of longitudinal flux tube waves (already used successfully in solar chromosphere models; see Herbold et al. 1985; Rammacher & Ulmschneider 1989; and Fawzy et al. 1998 for details). We considered two different flux tube geometries: uniformly distributed flux tubes and flux tubes arranged as a chromospheric network. The stellar photospheric filling factors, f_0, were chosen according to recent observations (see C98 for details), which allowed us to deduce a semiempirical relationship between the stellar rotation period $P_{\rm rot}$ and $B_0 f_0$, where B_0 is the average photospheric magnetic field strength. In this case, f_0 and the photospheric flux tube distribution constrained the shape of the tubes including their top opening radii.

We calculated models of K2 V stars with rotation rates between 10 and 40 days. Regarding the acoustic and magnetic energy fluxes, we used the results recently obtained by Ulmschneider et al. (1996) and Ulmschneider & Musielak (1998), respectively. We also considered contributions from mode coupling between transverse and longitudinal tube waves. The MHD flux tube calculations have been performed for thin magnetic flux tubes. We considered monochromatic waves for both acoustically and magnetically heated components. The calculated two-component chromosphere models have been used to compute the Ca II K emission flux based on multiray (1.5-dimensional) radiative transfer with partial redistribution (PRD), which was then converted into the Ca II H + K emission flux.

We found the following results:

1. Owing to the presence of magnetic flux tubes, the heating and chromospheric flux emission was found to be significantly larger in the magnetic component than in the nonmagnetic one. Magnetic heating was found to be strongest in flux tubes with the least spreading with height, expected to occur on rapidly rotating stars with high f_0.

2. The Ca II emission flux $F_{\rm HK}$ was calculated for stars with stellar rotation rates ranging from 10 to 40 days. We found that regardless of the flux tube distribution considered, the $F_{\rm HK}$ flux was the highest in the star with $P_{\rm rot} =$ 10 days and the lowest in the star with $P_{\rm rot} = 40$ days.

3. The theoretical $F_{\rm HK}$-$P_{\rm rot}$ relationship deduced for our K2 V star models was found to be consistent within 3 σ error bars with the empirical $F'_{\rm HK}$-$P_{\rm rot}$ relationship. For stars with $P_{\rm rot} \gtrsim 25$ days, no significant differences between the two flux tube distributions (i.e., uniformly distributed tubes and tubes arranged as a chromospheric network) were found. For stars with $P_{\rm rot} \lesssim 25$ days, however, the uniform model agreed better with observations, although this result needs to be checked with further modeling.

4. For stars with very low filling factors, i.e., stars with very slow rotation, we were able to reproduce the "basal flux limits" of chromospheric emission, which were previously attributed to pure acoustic heating (see B98 for details). Here we already have considered the new acoustic energy fluxes by Ulmschneider et al. (1996). This allows us to consider our two-component chromosphere models as a well-defined extension to one-component chromosphere models based on pure acoustic heating.

5. With the use of time-dependent two-component chromospheric (magneto-)acoustic heating models, it appears now possible to directly link the $B_0 f_0$-$P_{\rm rot}$ relationship to the $F_{\rm HK}$-$P_{\rm rot}$ relationship, which are both deduced from observations and are typical for a given type of stars.

6. Longitudinal tube waves produce Ca II H + K emission fluxes in agreement with observations, suggesting that wave heating is a sufficient chromospheric heating mechanism in magnetically active K stars with $P_{\rm rot} \geq 10$ days. Nonetheless, the relevance of such other mechanisms as, e.g., flare heating still needs to be checked.

7. Our models show remarkable behavior in the efficiency of converting the initial wave energy flux into Ca II radiation. Although the initial magnetic wave energy flux is almost 30 times greater than the initial acoustic wave

energy flux, the F_{HK} emission by the two-component chromosphere models is increased only by a factor of 1.5–4.5 relative to the nonmagnetic component. The reason is twofold: the magnetic wave energy flux is considerably reduced with height owing to the increase of the tube cross section, and the density inside the flux tubes is considerably lower than outside of the tubes, which leads to reduced Ca II radiative emission.

8. For the star with the highest f_0, we varied $P_{w,m}$ in the range between 30 and 90 s. We found that the differences in the Ca II emergent fluxes were marginal at best owing to the influence of Ca II–III ionization, which counteracts increased heating. This suggests that the theoretical F_{HK}-P_{rot} relationship may remain essentially unchanged when the monochromatic longitudinal tube waves are substituted by frequency spectra.

We consider these results as an important step toward a consistent theoretical explanation of chromospheric emission in stars of different types and levels of magnetic activity. Some technical improvements in our wave models, however, still need to be made, including using (magneto-) acoustic frequency spectra instead of monochromatic waves, the self-consistent treatment of mode coupling between longitudinal and transverse tube waves, and the simulation of line emission based on multilevel atoms. Also test computations with three-dimensional radiative transfer instead of multiray 1.5-dimensional radiative transfer should be performed to gauge the importance of radiative transfer effects. Additionally, we plan to target the following future projects: First, we want to expand our two-component chromospheric heating models to other types of stars, including main-sequence stars of different spectral types, subgiants, giants, and supergiants. In the past, a large number of observational data have been collected, which deserve to be evaluated by theoretical models. We thus should be able to gain insight into heating of multi-component atmospheres, the evolution of magnetic activity in the H-R diagram, the role of magnetic braking in chromosphere heating, and the appearance of HRD dividing lines. It would also be important to consider emission lines other than Ca II, including transition layer lines.

Although the best agreement between observations and theoretical models has been obtained for uniformly distributed flux tubes, particularly in case of fast rotating stars, this does not necessarily imply that flux tubes on K2 V stars are indeed uniformly distributed. We know for the Sun that homogeneous coverage does not occur: at cycle minimum, the concentrations are clearly arranged in a network, while at maximum a combination of magnetic plages and enhanced network is seen. The agreement of the emissions of the Sun as a star throughout its cycle with relationships between radiative flux densities from different stars appears to be in fact relying on the nonhomogeneous mixture of very active and inactive regions, including everything in between (Schrijver & Harvey 1989). We realize that temporal variations of the magnetic surface structure are also expected to occur in other types of stars including K dwarfs. This should motivate future research of radiative emission due to different mixtures of magnetic and nonmagnetic surface structure. The fact that uniform coverage of magnetic regions provides the best agreement between theoretical models and observations for fast rotating stars may indicate that a homogeneous coverage of plages in fast rotating K dwarf stars may dominate the chromospheric emission.

A further reason that radiative emission of nonuniform magnetic flux tubes distributions should be studied in more detail is the following: We know that numerous stars show rotational modulation of chromospheric emission attributable to distinct surface structures of increased heating, notably magnetic spots. It would be interesting to utilize theoretical models of dense spotlike flux tube distributions to assess chromospheric emission modulation observed in specific stars. An interesting example in that respect is the BY Dra star HD 82558, which is a single, rapidly rotating spotted K2 dwarf with a high magnetic activity level (Fekel et al. 1986). Saar, Piskunov, & Tuominen (1992) were able to derive both a temperature and magnetic field surface map and identified strong fields ($\overline{B} > 2$ kG) near cool spots (where $\Delta T_{eff} > 300$ K) and weaker fields with $\overline{B} \simeq 1$ kG elsewhere.

We would like to thank Jeff Hall for helpful discussions about the calibration of Ca II data and James J. Swain (UAH, College of Engineering) for support in the statistical data analysis. This work has been supported by the NASA Astrophysical Theory Program under NAG 5-3027 to the University of Alabama in Huntsville (M. C., P. U., and Z. E. M.), by NASA/MSFC under grant NAG 8-839 (Z. E. M.), by NSF under grants ATM 95-26196 (Z. E. M.) and AST 95-28563 (S. H. S.), and by NATO under grant CRG-910058 (P. U. and Z. E. M.). Z. E. M. also acknowledges support by the Alexander von Humboldt Foundation. We also would like to thank an anonymous referee for helpful comments.

APPENDIX A

THE TOP OPENING RADIUS OF FLUX TUBES

The top radii of flux tubes depend on the geometrical distribution of the flux tubes. Here we consider two cases: flux tubes that are uniformly distributed on the stellar surface and flux tubes arranged as a chromospheric network that is embedded in a nonmagnetic region. In the first case, the chromospheric magnetic filling factor beyond a certain height is identical to one because the flux tubes merge. In the second case, however, a decisive nonmagnetic component exists at all heights. To comply with this difference, different formulae for the flux tube top radii must be used.

Let us first we discuss the case of uniformly distributed tubes. With $F_{ph,m}$ being the magnetic photospheric area and F_T the total surface area, we have

$$F_{ph,m} = f_0 F_T = \pi r_0^2 ,$$

where r_0 denotes the photospheric tube radius and f_0 the magnetic filling factor at the photospheric level $\tau_{5000} = 1$. With $F_{\mathrm{ch},m}$ being the magnetic chromospheric area and r_∞ the tube top radius, we find $F_{\mathrm{ch},m} = 4r_\infty^2$ because the magnetic chromosphere formally consists of squares with inscribed circular flux tubes. Assuming that above a given height, the chromosphere is completely filled with flux tubes, i.e., $F_T = F_{\mathrm{ch},m}$, we find

$$r_\infty = 0.5 r_0 \sqrt{\pi / f_0} \, .$$

With respect to network tubes, we consider two modifications. First we assume $F_{\mathrm{ch},m} = \pi r_\infty^2$ consistent with C98. We also assume that the chromosphere is not entirely filled with flux tubes, i.e., that a nonmagnetic component remains even at large chromospheric heights. The chromospheric magnetic filling factor after the merging of the tubes is assumed to be 25%, which yields $F_{\mathrm{ch},m} = 0.25 F_T$. Hence we find

$$r_\infty = r_0 \sqrt{1/4 f_0} = r_0 \sqrt{1/f_N}$$

in agreement with C98. Here f_N denotes the magnetic filling factor for the chromospheric network. Note that f_N is identical to f_S (see § 2.1), if the area between the tubes, i.e., the difference between quadratic and circular tube expansion at the height of tube merging is disregarded. The top opening radii r_∞ for the different types of tubes is given in Table 1.

APPENDIX B

MHD EQUATIONS FOR LONGITUDINAL FLUX TUBE WAVES

To calculate longitudinal MHD flux tube models with different spatial filling factors, we consider vertically directed magnetic flux tubes embedded in a nonmagnetic atmosphere. Following Herbold et al. (1985), the MHD equations in the thin flux tube approximation can be written

$$\frac{\partial}{\partial t}\left(\frac{\rho}{B}\right) + \frac{\partial}{\partial z}\left(\frac{\rho u}{B}\right) = 0 \, , \tag{B1}$$

$$\frac{\partial u}{\partial t} + u \frac{\partial u}{\partial z} + \frac{1}{\rho}\frac{\partial p}{\partial z} + g = 0 \, , \tag{B2}$$

$$p + \frac{B^2}{8\pi} = p_e(z) \, , \tag{B3}$$

$$\frac{\partial S}{\partial t} + u \frac{\partial S}{\partial z} = \left.\frac{dS}{dt}\right|_{\mathrm{Rad}} \, . \tag{B4}$$

Here ρ is the density, p is the gas pressure, S is the entropy, u is the gas velocity, and B is the magnetic field strength in the tube. They are functions of height z and time t. p_e is the gas pressure outside the tube and is a function of z only. g is the stellar surface gravity, which is constant. The radiative damping function $dS/dt\,|_{\mathrm{Rad}}$ is computed following Ulmschneider et al. (1987) with modifications described by Buchholz et al. (1994).

The Alfvén speed c_{A} and tube speed c_T are given by $c_{\mathrm{A}} = B/(4\pi\rho)^{1/2}$ and $c_T^{-2} = c_S^{-2} + c_{\mathrm{A}}^{-2}$, respectively, where c_S denotes the adiabatic sound speed. The relationship between the thermodynamic variables is given by the ideal gas law $p/\rho = \Re T/\mu$ and $c_S^2 = \gamma \Re T/\mu$, where γ is the ratio of specific heats, μ is the molecular weight, and $\Re$ is the gas constant.

Considering the first and second laws of thermodynamics for an ideal gas, these equations can be written as a system of three partial differential equations for the three unknowns c_S, S, and u. To employ the method of characteristics, we transform this system of three partial differential equations into a system of six ordinary differential equations defined along the three characteristics C^+, C^-, and C^0. We obtain the compatibility relations

$$du \pm \frac{2}{\gamma - 1}\frac{c_S}{c_T}\, dc_S \mp \frac{\mu c_S}{\gamma \Re}\frac{c_S}{c_T}\, dS \mp \frac{\mu c_T (\gamma - 1)}{\gamma \Re}\left.\frac{dS}{dt}\right|_{\mathrm{Rad}} dt \mp \frac{u c_T}{\rho c_A^2}\frac{dp_e}{dz}\, dt + g dt = 0 \tag{B5}$$

along the C^+ and C^- characteristics given by

$$\frac{dz}{dt} = u \pm c_T \, , \tag{B6}$$

where the upper (lower) sign corresponds to the C^+ (C^-) characteristic. Equations (B5) and (B6) are four ordinary differential equations. The two remaining ordinary differential equations are obtained from equation (B4) written in characteristic form

$$dS = \left.\frac{dS}{dt}\right|_{\mathrm{Rad}} dt \tag{B7}$$

along the (fluid path) C^0 characteristic

$$\frac{dz}{dt} = u \, . \tag{B8}$$

To calculate the energy dissipation at the shocks, the MHD Rankine-Hugoniot relations for longitudinal tube waves are solved, which also allow for the different degrees of distensibility in the preshock and postshock regions. The method of solution involves a cubic equation that is solved by a Newton-Raphson iteration scheme (e.g., Fawzy et al. 1998).

APPENDIX C

CALIBRATION OF Ca II SURFACE FLUX OBSERVATIONS

There are two widely used methods of converting Mount Wilson $\langle S \rangle$ measurements (the sum of fluxes in a 1.09 Å wide triangular filter centered at the cores of the Ca II H and K lines, ratioed to the sum at two continuum points) into surface fluxes. The two use slightly different calibrations of the continuum flux, different $T_{\rm eff}$ scales, have different scaling constants, and subtract different color- (i.e., $T_{\rm eff}$) dependent "background" terms. These background fluxes account for residual flux in the core of the Ca II lines thought not to be of chromospheric origin—termed "photospheric" by Noyes et al. (1984) or "basal" by Rutten (1984).

Noyes et al. (1984) compute

$$R'_{\rm HK} = F'_H K/(\sigma T_{\rm eff}^4) = R_{\rm HK} - R_{\rm HK}({\rm phot}) ,$$

where

$$R_{\rm HK} = 1.340 \times 10^{-4} C_{\rm cf}(N) \langle S \rangle ,$$

and the continuum calibration term (Middelkoop 1982) is

$$\log C_{\rm cf}(N) = 1.13(B-V)^3 - 3.91(B-V)^2 + 2.84(B-V) - 0.47 + \delta(B-V) ,$$

with a correction term

$$\delta(B-V) = 0.135x - 0.814x^2 + 6.03x^3 ,$$

where $x = 0.63 - (B-V)$. The background term is given by

$$\log R_{\rm HK}({\rm phot}) = -4.898 + 1.918(B-V)^2 - 2.893(B-V)^3 .$$

Noyes et al. (1984) use a fit to the Johnson (1966) $T_{\rm eff}$ scale: $\log T_{\rm eff} = 3.908 - 0.234(B-V)$. The surface flux is then given by

$$F'_{\rm HK} = R'_{\rm HK}(\sigma T_{\rm eff}^4) .$$

The Rutten (1984) calibration computes:

$$\Delta F_{\rm HK} = F_{\rm HK} - F_{\rm HK}({\rm basal}) ,$$

where

$$F_{\rm HK} = 10^{-14} K C_{\rm cf}({\rm RS}) T_{\rm eff}^4 \langle S \rangle ,$$

and the continuum calibration term is an improved version of Middelkoop's (1982) given by

$$\log C_{cf}({\rm RS}) = 0.25(B-V)^3 - 1.33(B-V)^2 + 0.43(B-V) + 0.24$$

and $K = 1.29 \times 10^6$ (Rutten 1987). The empirical "basal" flux, $F_{\rm HK}$(basal), is derived from the minimum $\langle S \rangle$ observed as a function of $B-V$; we interpolated $F_{\rm HK}$(basal) from the table in Rutten (1987). For consistency, we used the same $T_{\rm eff}$ scale as Noyes et al. (1984)—Rutten used a slightly different scale (from Böhm-Vitense 1981). The differences in $\log C_{\rm cf}$ are less than ± 0.02 dex for $0.55 \leq B-V \leq 1.40$; however, $F_{\rm HK}$(basal) $> F_{\rm HK}$(phot) throughout this interval, with differences minimized near $(B-V)_\odot$ and increasing for larger and smaller values (e.g., Rutten 1986).

Unfortunately, the two calibrations do not agree well, particularly for active stars where differences should be minimized (disagreements about the background correction are small relative to the total flux in active stars). Part of the problem is discussed by Hall & Lockwood (1995), who argue that $K = 7.97 \times 10^5$ is a more accurate scaling constant (and closer to Middelkoop's original value of 7.6×10^5). Because of the residual questions about the Rutten calibration, however, we have preferred to compare our models to fluxes computed using the Noyes et al. (1984) method. We leave open the possibility that it may be advantageous to employ an altered version of the Rutten calibration, with its conceptually useful $F_{\rm HK}$(basal), at some future point.

REFERENCES

Ayres, T. R., Simon, T., Stauffer, J. R., Stern, R. A., Pye, J. P., & Brown, A. 1996, ApJ, 473, 279
Baliunas, S. L., et al. 1983, ApJ, 275, 752
———. 1995, ApJ, 438, 269
Baliunas, S. L., Nesme-Ribes, E., Sokoloff, D., & Soon, W. H. 1996, ApJ, 460, 848
Basri, G., Marcy, G. W., & Valenti, J. A. 1990, ApJ, 360, 650
Böhm-Vitense, E. 1981, ARA&A, 19, 295
Buchholz, B., Hauschildt, P., Rammacher, W., & Ulmschneider, P. 1994, A&A, 285, 987
Buchholz, B., Ulmschneider, P., & Cuntz, M. 1998, ApJ, 494, 700 (B98)
Bünte, M., Steiner, O., & Pizzo, V. J. 1993, ApJ, 268, 299
Carlsson, M., & Stein, R. F. 1992, ApJ, 397, L59
Cattaneo, F., Brummell, N. H., Toomre, J., Malagoli, A., & Hurlburt, N. E. 1991, ApJ, 370, 282
Char, S., Foing, B. H., Beckman, J., García López, R. J., & Rebolo, R. 1993, A&A, 276, 78
Charbonneau, P., Schrijver, C. J., & MacGregor, K. B. 1997, in Cosmic Winds and the Heliosphere, ed. J. R. Jokipii et al. (Tucson: Univ. of Arizona Press), 677
Cuntz, M., & Höflich, P. 1999, in preparation
Cuntz, M., & Muchmore, D. O. 1994, ApJ, 433, 303

Cuntz, M., Ulmschneider, P., & Musielak, Z. E. 1998, ApJ, 493, L117 (C98)
Donahue, R. A., Saar, S. H., & Baliunas, S. L. 1996, ApJ, 466, 384
Durney, B. R., de Young, D. S., & Roxburgh, I. W. 1993, Sol. Phys. 145, 207
Fawzy, D. E., Ulmschneider, P., & Cuntz, M. 1998, A&A, 336, 1029
Fekel, F. C., Bopp, B. W., Africano, J. L., Goodrich, B. D., Palmer L. H., Quigley, R., & Simon, T. 1986, AJ, 92, 1150
Fleck, B., & Schmitz, F. 1993, A&A, 273, 671
Gouttebroze, P. 1986, A&A, 160, 195
Gray, D. F. 1989, ApJ, 347, 1021
Hall, J. C., & Lockwood, G. W. 1995, ApJ, 438, 404
Hasan, S. S., & van Ballegooijen, A. A. 1998, in ASP Conf. Ser. 154, Cool Stars, Stellar Systems, and the Sun X, ed. R. A. Donahue & J. A. Bookbinder (San Francisco: ASP), 630
Herbold, G., Ulmschneider, P., Spruit, H. C., & Rosner, R. 1985, A&A, 145, 157
Hoffleit, D., & Jascheck, C. 1982, The Bright Star Catalogue (4th ed.; New Haven: Yale Univ. Obs.)
Huang, P., Musielak, Z. E., & Ulmschneider, P. 1995, A&A, 279, 579
———P. 1999, A&A, 342, 300
Johnson, H. R. 1966, ARA&A, 4, 193
Jordan, C. 1997, Astron. Geophys., 38 (2), 10
Keppens, R., MacGregor, K. B., & Charbonneau, P. 1995, A&A, 294, 469
Kraft, R. P. 1967, ApJ, 150, 551
Marcy, G. W., & Basri, G. 1989, ApJ, 345, 480
Middelkoop, F. 1982, A&A, 107, 31
Montesinos, B., & Jordan, C. 1993, MNRAS, 264, 900
Montgomery, D. C., & Peck, E. A. 1992, Introduction to Linear Regression Analysis (2d ed.; New York: John Wiley)
Mullan, D. J., & Cheng, Q. Q. 1993, ApJ, 412, 312
Musielak, Z. E., Rosner, R., Gail, H.-P., & Ulmschneider, P. 1995, ApJ, 448, 865
Musielak, Z. E., Rosner, R., Stein, R. F., & Ulmschneider, P. 1994, ApJ, 423, 474
Narain, U., & Ulmschneider, P. 1990, Space Sci. Rev., 54, 377
———. 1996, Space Sci. Rev., 75, 453
Nordlund, Å., & Dravins, D. 1990, A&A, 228, 155
Noyes, R. W., Hartmann, L. W., Baliunas, S. L., Duncan, D. K., & Vaughan, A. H. 1984, ApJ, 279, 763
Rammacher, W., Ulmschneider, P., & Cuntz, M. 1999, in preparation
Rammacher, W., & Cuntz, M. 1991, A&A, 250, 212
Rammacher, W., & Ulmschneider, P. 1989, in Solar and Stellar Granulation, ed. R. J. Rutten & G. Severino (Dordrecht: Kluwer), 589
———. 1992, A&A, 253, 586
Rast, M. P., & Toomre, J. 1993, ApJ, 419, 240
Roberts, B. 1991, in Advances in Solar System Magnetohydrodynamics, ed. E. R. Priest & A. W. Hood (Cambridge: Cambridge Univ. Press), 105
Rosner, R., Musielak, Z. E., Cattaneo, F., Moore, R. L., & Suess, S. T. 1995, ApJ, 442, L25
Rüedi, I., Solanki, S. K., Mathys, G., & Saar, S. H. 1997, A&A, 318, 429
Rutten, R. G. M. 1984, A&A, 130, 353
———. 1986, A&A, 159, 291
———. 1987, A&A, 177, 131
Rutten, R. G. M., & Pylyser, E. 1988, A&A, 191, 227
Rutten, R. G. M., Schrijver, C. J., Lemmens, A. F. P., & Zwaan, C. 1991, A&A, 252, 203
Saar, S. H. 1996a, in IAU Symp. 176, Stellar Surface Structure, ed. K. G. Strassmeier & J. L. Linsky (Dordrecht: Kluwer), 237
Saar, S. H. 1996b, in IAU Colloq. 153, Magnetodynamic Phenomena in the Solar Atmosphere—Prototypes of Stellar Magnetic Activity, ed. Y. Uchida et al. (Dordrecht: Kluwer), 367
———. 1998, in ASP. Conf. Ser. 154, Cool Stars, Stellar Systems, and the Sun X, ed. R. A. Donahue & J. A. Bookbinder (San Francisco: ASP), 211
Saar, S. H., & Baliunas, S. L. 1992, in ASP Conf. Ser. 27, The Fourth Solar Cycle Workshop, ed. K. L. Harvey (San Francisco: ASP), 197
Saar, S. H., Bünte, M., & Solanki, S. K. 1994, in ASP Conf. Ser. 64, Cool Stars, Stellar Systems, and the Sun VIII, ed. J.-P. Caillault (San Francisco: ASP), 474
Saar, S. H., Piskunov, N. E., & Tuominen, I. 1992, in ASP Conf. Ser. 26, Cool Stars, Stellar Systems, and the Sun VII, ed. M. S. Giampapa & J. A. Bookbinder (San Francisco: ASP), 255
Saar, S. H., & Schrijver, C. J. 1987, in Cool Stars, Stellar Systems, and the Sun V, ed. J. L. Linsky & R. E. Stencel (Berlin: Springer), 38
Schmitt, J. H. M. M. 1997, A&A, 318, 215
Schmitz, F., Ulmschneider, P., & Kalkofen, W. 1985, A&A, 148, 217
Schrijver, C. J. 1987, A&A, 172, 111
———. 1995, A&ARev., 6, 181
———. 1996, in IAU Symp. 176, Stellar Surface Structure, ed. K. G. Strassmeier & J. L. Linsky (Dordrecht: Kluwer), 1
Schrijver, C. J., Coté, J., Zwaan, C., & Saar, S. H. 1989, ApJ, 337, 964
Schrijver, C. J., & Harvey, K. L. 1989, ApJ, 343, 481
Schrijver, C. J., & Pols, O. R. 1993, A&A, 278, 51
Schrijver, C. J., et al. 1998, Nature, 394, 152
Simon, T., & Drake, S. A. 1989, ApJ, 346, 303
Simon, T., Herbig, G., & Boesgaard, A. M. 1985, ApJ, 293, 551
Skumanich, A. 1972, ApJ, 171, 565
Solanki, S. K. 1996, in IAU Symp. 176, Stellar Surface Structure, ed. K. G. Strassmeier & J. L. Linsky (Dordrecht: Kluwer), 201
Solanki, S. K., Steiner, O., & Uitenbroeck, H. 1991, A&A, 250, 220
Soon, W. H., Baliunas, S. L., & Zhang, Q. 1994, Sol. Phys., 154, 385
Steiner, O., Grossmann-Doerth, U., Schüssler, M., & Knölker, M. 1996, Sol. Phys., 164, 223
Stępień, K., & Ulmschneider, P. 1989, A&A, 216, 139
Strassmeier, K. G., Handler, G., Paunzen, E., & Rauth, M. 1994, A&A, 281, 855
Sutmann, G., & Ulmschneider, P. 1995, A&A, 294, 241
Theurer, J. 1998, Ph.D. thesis, Univ. Heidelberg
Ulmschneider, P. 1970, Sol. Phys., 12, 403
———. 1986, A&A, 168, 308
———. 1994, A&A, 288, 1021
Ulmschneider, P., Kalkofen, W., Nowak, T., & Bohn, H. U. 1977, A&A, 54, 61
Ulmschneider, P., Muchmore, D., & Kalkofen, W. 1987, A&A, 177, 292
Ulmschneider, P., & Musielak, Z. E. 1998, A&A, 338, 311
Ulmschneider, P., Musielak, Z. E., & Fawzy D. E. 1999, in preparation
Ulmschneider, P., Schmitz, F., Kalkofen, W., & Bohn, H. U. 1978, A&A, 70, 487
Ulmschneider, P., Theurer, J., & Musielak, Z. E. 1996, A&A, 315, 212
Ulmschneider, P., Zähringer, K., & Musielak, Z. E. 1991, A&A, 241, 625
Valenti, J. A., Marcy, G. W., & Basri, G. 1995, ApJ, 439, 939
Vaughan, A. H., Preston, G. W., & Wilson O. C. 1978, PASP, 90, 267
Walter, F. M. 1996, in IAU Symp. 176, Stellar Surface Structure, ed. K. G. Strassmeier & J. L. Linsky (Dordrecht: Kluwer), 355
Wilson, O. C. 1966, ApJ, 144, 695
Wilson, O. C., & Skumanich, A. 1964, ApJ, 140, 1401